sensors

Article

A Novel Spinel Ferrite-Hexagonal Ferrite Composite for Enhanced Magneto-electric Coupling in a Bilayer with PZT

Sujoy Saha [1], Sabita Acharya [1], Maksym Popov [1,2], Theodore Sauyet [3], Jacob Pfund [3], Rao Bidthanapally [1], Menka Jain [3], Michael R. Page [4] and Gopalan Srinivasan [1,*]

[1]Department of Physics, Oakland University, Rochester, MI 48309, USA
[2]Institute of High Technologies, Taras Shevchenko National University of Kyiv, Kyiv, Ukraine
[3]Department of Physics, University of Connecticut, Storrs, Connecticut 06269, USA
[4] Materials and Manufacturing Directorate, Air Force Research Laboratory, Wright-Patterson Air Force Base, Dayton, Ohio 45433, USA
* Correspondence: Corresponding author: Gopalan Srinivasan, email: srinivas@oakland.edu

Abstract: The magnetoelectric effect (ME) is an important strain mediated phenomenon in a ferromagnetic-piezoelectric composite for a variety of sensors and signal processing devices. A bias magnetic field, in general, is essential to realize a strong ME coupling in most composites. Magnetic phases with (i) high magnetostriction for strong piezomagnetic coupling and (ii) large anisotropy field that acts as a built-in bias field are preferred so that miniature, ME composite-based devices can operate without the need for an external magnetic field. We are able to realize such a magnetic phase with a composite of (i) barium hexaferrite (BaM) with high magnetocrystalline anisotropy field and (ii) nickel ferrite (NFO) with high magnetostriction. The BNx composites, with (100-x) wt.% of BaM and x wt.% NFO, for x = 0-100, were prepared. X-ray diffraction analysis shows that the composites did not contain any impurity phases. Scanning electron microscopy images revealed that with an increase in NFO content, hexagonal BaM grains become prominent, leading to a large anisotropy field. The room temperature saturation magnetization showed a general increase with increasing BaM content in the composites. NFO rich composites with x ≥60 were found to have a large magnetostriction value of around -23 ppm, comparable to pure NFO. The anisotropy field H_A of the composites, determined from magnetization and ferromagnetic resonance (FMR) measurements, increased with increasing NFO content and reached a maximum of 7.77 kOe for x= 75. The BNx composite was cut into rectangular platelets and bonded with PZT to form the bilayers. ME voltage coefficient (MEVC) measurements at low frequencies and at mechanical resonance showed strong coupling at zero bias for samples with x ≥33. This large in-plane H_A acted as a built-in field for strong ME effects under zero external bias in the bilayers. The highest zero-bias MEVC of ~22 mV/cm Oe was obtained for BN75-PZT bilayers wherein BN75 also has the highest H_A. Bilayer of BN95-PZT showed a maximum MEVC ~992 mV/cm Oe at electromechanical resonance at 59 kHz. The use of hexaferrite-spinel ferrite composite to achieve strong zero-bias ME coupling in bilayers with PZT is significant for applications related to energy harvesting, sensors, and high frequency devices.

Keywords: Magnetoelectric; Spinel Ferrite; Hexagonal ferrite; Ferroelectric; Composite.

1. Introduction

Multiferroic materials exhibit more than one ferroic order, such as ferromagnetism, ferroelectricity, and ferroelasticity [1]. They have recently attracted significant attention due to their potential for applications in spintronics, magneto-electrics, nonvolatile memories, sensors, and electrically tunable magnetic microwave devices [2,3]. A ferromagnetic-ferroelectric composite is a multiferroic that shows a variation of its ferroelectric order parameters when subjected to an external magnetic field, direct magnetoelectric (ME) effect, or changes in magnetic parameters in an applied electric field, converse ME effect. [4]. In ME materials, the induced electric polarization P is related to the applied external magnetic field H by P = α H, where α is a second order ME-susceptibility tensor. Another parameter of importance is the ME voltage coefficient (MEVC) $\alpha_E = \delta E/\delta H$, where δE is the induced electric field due to applied magnetic field δH, and is related to α by $\alpha = \varepsilon_0\varepsilon_r\alpha_E$, where ε_r is the relative permittivity of the material. According to models for the ME effects in single-phase materials, the upper bound α is limited to the relation $\alpha \leq (\mu\varepsilon)^{1/2}$, where μ and ε are the permeability and permittivity of the material, respectively [5]. One of the known single-phase multiferroic with a large α at room temperature is $BiFeO_3$ [6]. In composite ME materials, α can be enhanced by exploiting the strain mediated interactions between the two phases [4].

To obtain the maximum ME voltage coefficient (α_E) in a ferromagnetic-ferroelectric composite an optimized magnitude of the DC magnetic bias field H is needed. A maximum in the α_E occurs when the piezomagnetic coefficient q = dλ/dH (where λ is the magnetostriction) of ferro/ferrimagnetic component of the composite is also maximum. Hence a bias magnetic field, in general, is essential to achieve a strong ME response. The need for a bias field, however, could be eliminated with a self-bias in the ferromagnetic. There are several avenues to accomplish the self-bias condition such as a large magneto-crystalline anisotropy field or the use of a functionally graded ferromagnet [7-9]. Other avenues include the use of compositionally graded ferromagnetic phase [10]. There are several experimental findings [11-13] and theoretical models [11-13] on graded ME composites. In laminated composites changing the mechanical resonance modes through electrical connectivity evoke the zero bias coupling when the bending strain activates a built-in bias [9]. Thin films that rely on magnetic field dependence of resonant frequency and angular dependence of exchange bias field [14, 15] can also show zero-bias ME effect. It is also shown that a homogeneous magnetostrictive phase can also produce zero bias ME effect [16]. Cofired layered composites consisting of textured $Pb(Mg_{1/3}Nb_{2/3})O_3$-$PbTiO_3$ (PMN-PT) and Cu and Zn doped $NiFe_2O_4$ show a giant zero-bias ME coefficient ~1000 mV/cm Oe [17] wherein built in stress induces zero-bias effect. Very recently Huang et. al. [18] have shown very large self-bias ME effect with $LiNbO_3$ single crystal and Ni trilayers with residual stress engineering by using Ni as electrode and piezomagnetic layer simultaneously using RF sputtering. Wu et. al. [19] have shown that large sensitivity in PMN-PT-Metglass ME sensors by utilizing shear stress induced self-bias effect. Annapureddy et. al. [20] have obtained large self-bias effect (~4200 mV/cmOe) by utilizing the graded magnetization. To date all the reported self-bias effect are sample specific. The role of the sample configuration and/or preparation is crucial to obtain the self-bias.

This work focuses on a novel, never-before used approach for a self-biased ME composite with the use of a ferromagnetic layer consisting of both M-type barium ferrite hexagonal ferrite, BaO $6Fe_2O_3$ (BaM), with uniaxial anisotropy on the order of ~ 17.4 kOe, and nickel ferrite $NiFe_2O_4$ with high magnetostriction and piezomagnetic coefficient q [21]. Composites of BaM-NFO with (100-x) wt.% of BaM and x wt.% of NFO, (BNx), were prepared by sintering powders of both ferrites. X-ray diffraction revealed the presence of both BaM and NFO and the absence of impurity phases. Scanning electron microscopy images showed crystallites of both ferrites. Magnetization measurements at room temperature for static fields up to 2 T showed an increase in $4\pi M$ with increasing BaM content in the composite. Magnetostriction λ measurements for BNx indicated an increase with increasing x and for x > 65 reached values comparable that of pure NFO. High frequency measurements were carried out to determine the anisotropy field H_A from dependence of the ferromagnetic resonance (FMR) frequency f_r on static magnetic field H. The in-plane H_A values in BNx were found to be well above the value of 500 Oe for pure NFO. These composites show a large piezomagnetic coefficient and large magnetocrystalline anisotropy simultaneously which is somewhat unique to this spinel ferrite-hexaferrite composite. Platelets of sintered BNx were bonded to PZT to form bilayers for ME voltage coefficient (MEVC) measurements that showed a significant zero-field ME effects. Details on results of the studies are provided in the following sections.

2. Experiment

2.1. Materials

The ferrite composites were prepared by the traditional ceramic synthesis techniques. Micrometer sized polycrystalline powders of NFO and BaM were first synthesized separately. High purity NiO, $BaCO_3$, and Fe_2O_3 were mixed and ballmilled for 8 h. The powders were dried and pre-sintered at 900 ºC for 6 h. The pre-sintered powders were ballmilled again and then sintered at 1200 ºC for 6 h. Composites of (100-x) wt.% BaM- x wt% NFO (BNx) (x=5, 9, 13, 33, 38, 41, 44, 47, 60, 75, 85 and 95) were prepared by mixing the ferrite powders. A binder, 2% PVA, was added to the powder and pressed into disks (diameter~18 mm and thickness ~2 mm) by applying uniaxial pressure of 250 MPa. The disks of BNx were finally sintered at 1250 ºC for 6 h.

2.2. Characterizations

The crystal structure of the composites was characterized by a powder X-ray diffractometer (Miniflex, Rigaku) at room temperature. Morphological features of the samples were studied with an SEM (JSM-6510/GS, JEOL). Magnetostriction of the composite on rectangular platelets were measured using a strain gage and a strain indicator/recorder (P3, Micro-Measurements). The magnetic field was applied parallel to the sample plane and along the length (direction-*1*) of the gage and magnetostriction measured in this configuration is labeled λ_{11}. Magnetization at room temperature as a function of H was measured with an Evercool Physical Property Measurement System (PPMS, Quantum Design Inc.). Ferromagnetic resonance (FMR) measurements were done on thin rectangular platelets of the composites with the sample placed on a coplanar waveguide and with the magnetic field H parallel to the sample plane and along its length. A vector network analyzer (Agilent) was used to record profiles of the scattering matrix S_{21} vs frequency f for a series of H. Measurements of ME coupling strengths were done on bilayer of BNx and vendor supplied PZT that was bonded with a thin layer of epoxy. Composite platelets of dimensions 10 mm x 5 mm and 1 to 1.5 mm in thickness and 0.3 mm thick PZT plates of similar lateral dimensions as the composite were used. The ME voltage coefficient (MEVC) measurements were done by subjecting the bilayer to an ac magnetic field H_{ac} and a bias field H. Both H- and f-dependence of the MEVC were measured for both the magnetic fields parallel each other and either parallel or perpendicular to the sample plane.

3. Results

3.1. Structural Characterization

Representative powder X-ray diffraction (XRD) patterns for the BNx samples are shown in Fig. 1. XRD patterns of other BNx compositions are shown in the Fig. S1 in the Supplement. The XRD patterns show diffraction peaks from NFO and BaM. With increasing x-values, the NFO lines become stronger and BaM lines get weaker as expected. This is due to the reduced weight fraction of the BaM phase as we increase x. X-ray intensity corresponding to a particular phase is proportional to the weight fraction of the phase. We have deliberately varied the weight fraction of the NFO/BaM phases and when the NFO weight fraction is increased the line intensity corresponding to NFO becomes stronger, likewise BaM intensity gets weaker. A small amount of an impurity phase, identified as antiferromagnetic $Ba_5Fe_2O_8$, is present only in BN41, BN44 and BN75 [22]. Usually, $Ba_5Fe_2O_8$ type impurities ($5BaO+Fe_2O_3$) occur during the sintering of BaO and Fe_2O_3 based ferrites, especially in $BaFe_{12}O_{19}$ [22]. However, since $Ba_5Fe_2O_8$ is antiferromagnetic, the overall ME character of the BNx-PZT bilayers is expected to be unaffected.

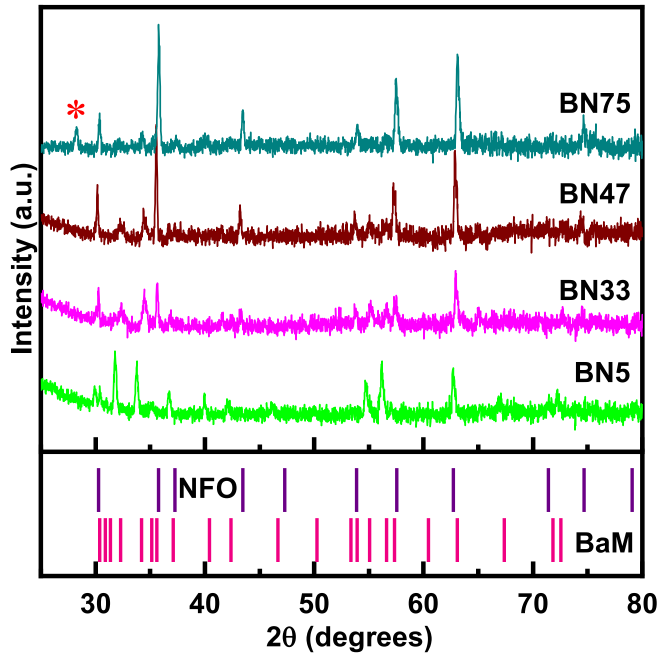

Figure 1. Representative X-ray diffraction data for BNx composites. All the composites bear the signatures of NFO and BaM. The stick patterns for NFO and BaM are shown in the bottom pane to visualize the one-to-one correspondence of the Braggs positions of each phase to the respective NFO and BaM lines. BN75 contains a small amount of an impurity phase, $Ba_5Fe_2O_8$, and is denoted by a star.

Representative SEM images for BNx (x=5, 33, 60 and 95) are shown in Fig. 2. The gradual increase in the grain size in the BN composites with increasing x (also in Supplementary Fig. S2) may indicate that NFO aids in the growth of hexagonal BaM grains for x≥9. Large grains are absent in BN5, but a closer examination of the surface morphology shows hexagonal-like features with grain size less than 2 μm. With increasing NFO content grains larger than 5 μm are present. For x > 41, the number of large grains reduces again. For the highest content of NFO (BN95) we observe a similar grain distribution as pure NFO (Supplementary Fig. S2). BN5 also shows a similar grain distribution as pure BaM. When the weight fraction of the BaM phase is high (x~5) the composite is more likely to behave as pure BaM. Hence the corresponding morphological features of composites with high BaM content should also look like pure BaM. Similarly, when the weight fraction (x>41) of NFO is increased the composites tends to show a reduction in BaM grains. Barium ferrite itself tends to form hexagonal grains [23] and with a tweak in the synthesis process the particle shape can be made nearly spherical [24]. In our case the processing has a large impact on the grain growth on these composites. The stabilization of the typical hexagonal BaM grains amongst NFO particles is worth noting.

The XRD results in Fig.1 and the SEM images of Fig.2 are just indicators of the absence of any significant amount of impurity phases of crystal structurs apart from spinel and hexagonal phases. An indepth investigation and analysis of the crystal and magnetic structures are in order. For example, possible migration of Ni-ion from the spinel phase to the hexagonal phase has to be addressed since the M-type hexagonal phase also has the spinel blocks as well. Such an investigation, however, is not the primary focus of this particular study.

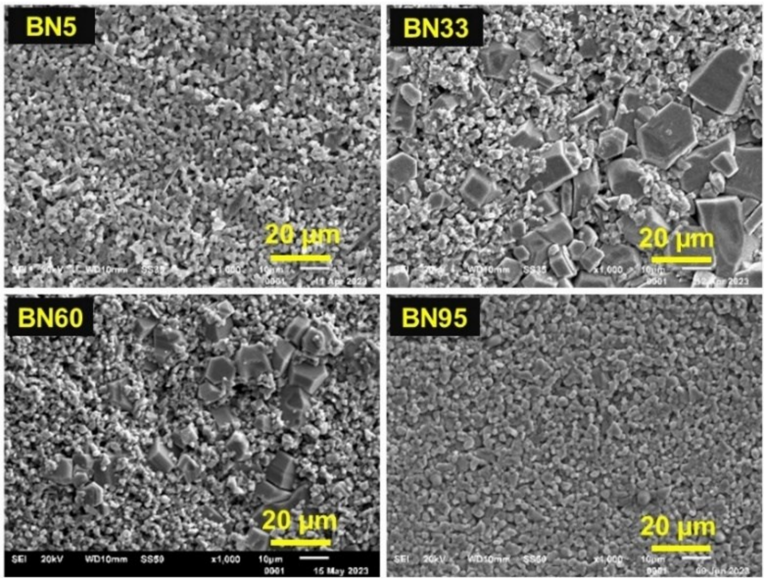

Figure 2. SEM images for BN5, BN33, BN60 and BN95 composites. There are no notable features in the image for BN5. Well defined hexagonal grains corresponding to the BaM phase is seen in BN33 and BN60. BN95 does not show any hexagonal grain.

3.2 Magnetic characterization

We have carried out room-temperature measurements of the magnetization, 4πM, of the composites as a function of applied magnetic field H. Representative 4πM vs H data are shown in Fig. 3 and Fig. S3. The M vs H loops show hysteresis and remanence as expected and the saturation values of M increases with increasing BaM contents in the composites. The H-values for saturation of the magnetization is less than 3 kOe for composites for NFO rich composites and it increases with increasing the amount of BaM. The magnetization 4πM at H=20 kOe increases from 2.90 kG for BN95 to 4 kG for BN33. The highest value of remanent 4πM of 1.04 kG was measured for BN75.

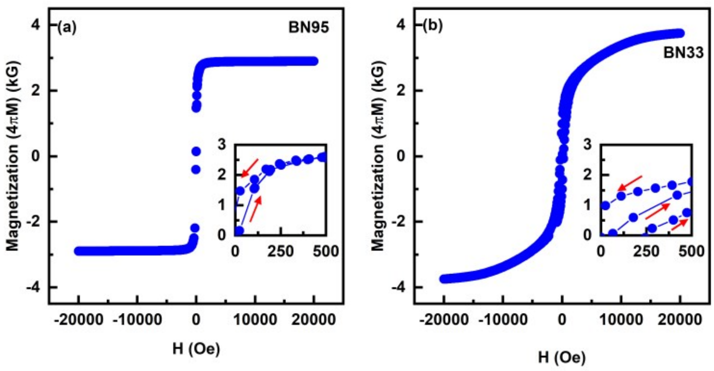

Figure 3. Room-temperature magnetization 4πM vs. magnetic field H data for (a) BN95 and (b) BN33 samples. The insets for low H-values clearly show the expected hysteresis and remanence in the M vs H data.

Since the magnetostriction λ is one of the key parameters that determine the strength ME interaction, we measured its value for the BNx composites. The measurements were done with a strain gage and a strain indicator and for H applied parallel to the sample plane and to the length of the strain gage. Data on the magnetostriction λ_{11} vs H are shown in Fig.4. The samples exhibit negative values for λ_{11} as expected since both NFO an BaM have negative λ_{11} values [25,26]. None of the λ_{11} values for the composites in Fig.3 show saturation for the maximum H-values of ~ 3 kOe. With increase in the NFO content λ_{11} values at 3 kOe increases and tends to show similar behavior as pure NFO (shown in the inset of Fig. 4). The highest value of λ_{11} ~ -23 ppm was measured for BN60 and we got similar values for x≥60. Our measurements on pure BaM showed λ_{11}=-1 ppm at 2.7 kOe. Hence it is clear that NFO phase is the major contributor towards the net magnetostriction of BNx composites.

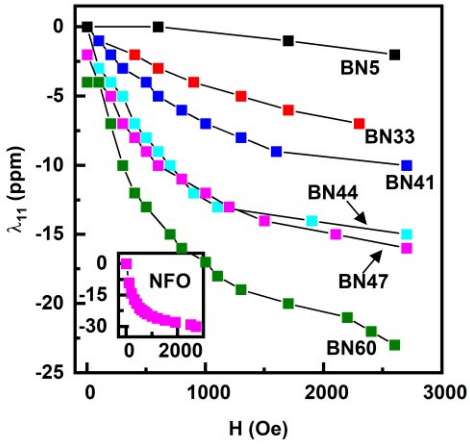

Figure 4. Magnetostriction, λ_{11} vs H data measured parallel to the in-plane H for BNx composites. The magnetic field was applied parallel to the length of the sample and the strain gage. λ_{11} for pure NFO is shown in the inset.

3.3 Ferromagnetic resonance

A key objective of this work is to achieve large enough magneto-crystalline anisotropy field H_A in BNx in order to realize a strong zero-bias ME effects in a composite with PZT. The magnetization data in Fig.3 and Fig.S3 do indicate a large remnant magnetization, as high as 1 kG, that is a clear evidence for a large H_A. We utilized ferromagnetic resonance (FMR) studies in combination with the magnetization data to determine H_A. Ferrite platelets, rectangular in shape, were placed in an S-shaped coplanar waveguide and excited with microwave power from a VNA. Profiles of the scattering matrix S_{21} as a function of frequency f were recorded. Figure 5 shows such profiles for a series of in-plane H along the sample length. For x values < 10, a single resonance mode was seen in the 50 GHz range (See Supplementary Fig. S4). With increasing NFO content two resonance modes were seen as in Fig. 5, one in the frequency range 3-20 GHz and another in the range 40-60 GHz. The S_{21} vs f profiles in Fig.5 (and Fig.S4) show clear asymmetry in the shape of the resonance absorption signals that can be attributed to the variations in the magnitudes of coupling between resonator and the transmission line at frequencies below and above the resonance. Such an asymmetry is not generally observed in cavity-type FMR measurements at a fixed frequency. Also, this effect is negligible for resonance modes with relatively narrow linewidth. However, for the case of transmission line broadband measurement systems and resonances with frequency-width on the order of a few GHz the asymmetry may manifest. Another possible factor is the frequency-dependent background absorption of the coplanar line which superimposes on absorption by the resonator and leads to significant distortion of the resultant profile. Such asymmetry is most likely occur at U-band frequencies, where any imperfections of stripline, connectors, or shielding may unpredictably affect the shape of stripline transmission characteristics. The resonance frequency was estimated from frequency of maximum absorption in the profiles in Fig.5. As discussed, next, the resonance mode at the low frequency region in Fig. 5 is due to FMR in NFO whereas the higher frequency resonance is a magneto-dielectric mode in the composite [27].

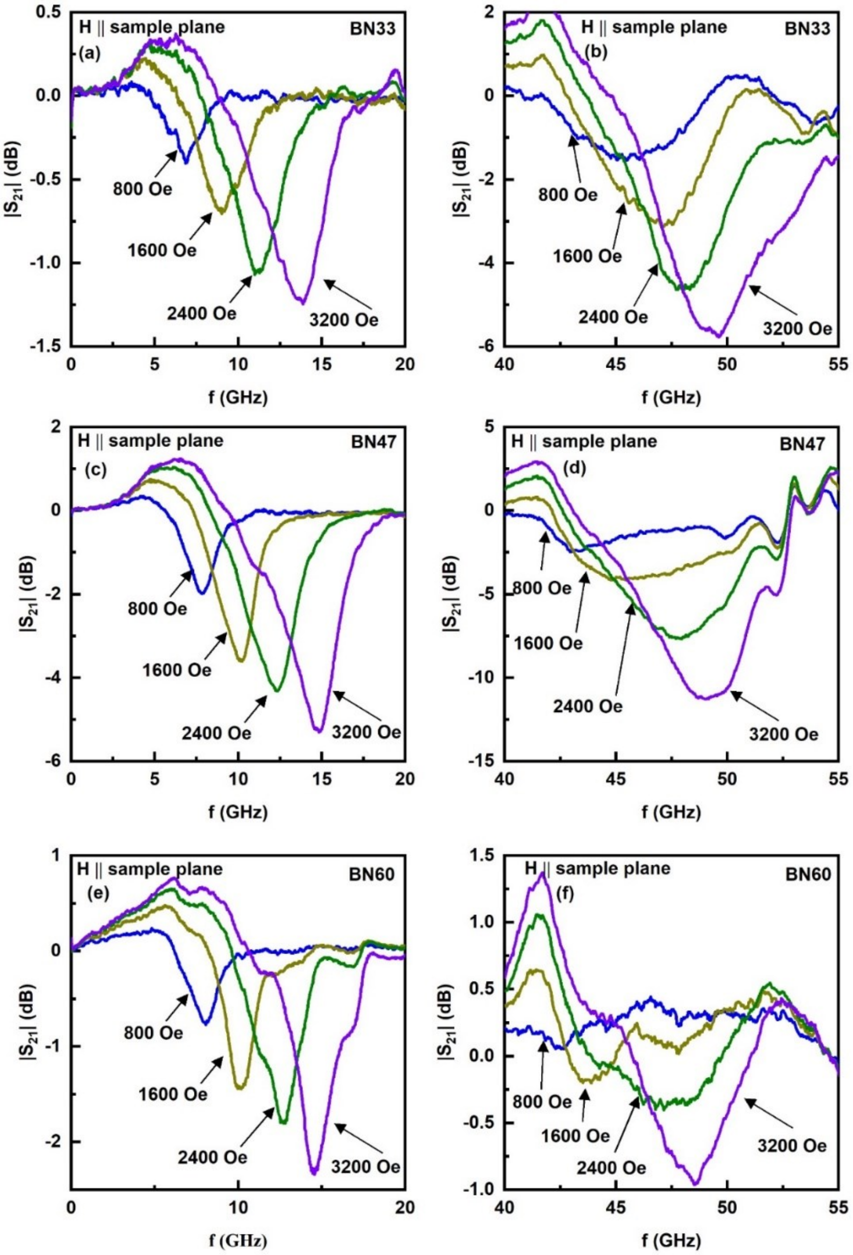

Figure 5. Profiles of S_{21} vs f showing resonances in BN33, BN47, and BN60 composites for in-plane static magnetic fields. The absorption in the profiles in Fig.5(a), (c) and (e) for 5-20 GHz is due to ferromagnetic resonance in NFO contents of BNx. Profiles in Fig.5 (b), (d) and (f) show absorption due to a magneto-dielectric mode in the composites.

The H-dependence of the low- and high frequency mode frequencies f_r are shown in Fig. 6 (and in Supplementary Fig. S5). Data on f_r vs H for the low-frequency mode are shown in Fig.6(a) for BN33 and BN60. With f_r increasing from 8.6 GHz at H= 1 kOe to 15.9 GHz for H=3.5 kOe for BN60 which amounts to an increase in f_r at the rate 2.8 GHz/kOe. A similar rapid increase in f_r with H is seen in Fig.6(a) for BN33. From the rate of change in f_r with H one may associate this mode with FMR in NFO. Data in Figure 6(b) on f_r vs H for the high frequency mode are for BN33 and BN60. This mode in Fig.5 and Fig.S5 shows a variation in f_r with H that could be approximated to a linear increase ~1.3 GHz/kOe. This slow variation in f_r with H is indicative of a magneto-dielectric mode in the composite platelet. This mode is not of importance for the current study and is not considered for further analysis [27].

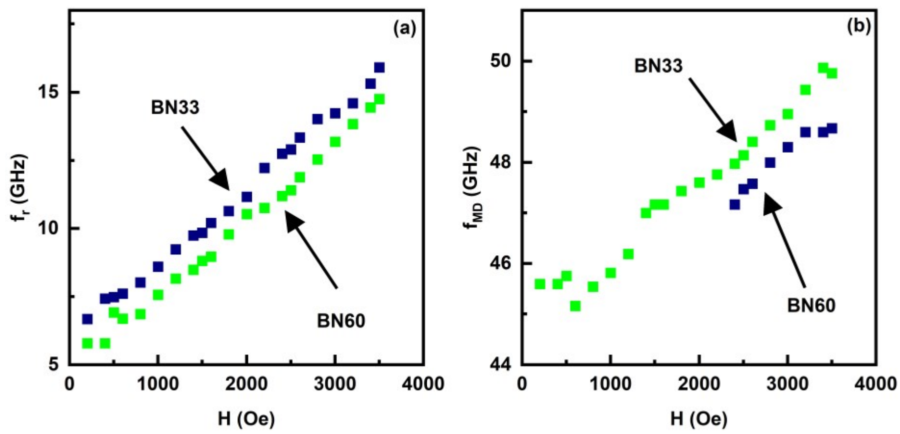

Figure 6. Ferromagnetic resonance frequency f_r as a function of H for (a) FMR observed in the low frequency region in Fig.5 and (b) magneto-dielectric mode frequency vs H for BNx composites.

The built-in bias due to magnetic anisotropy field H_A in the composites is a key parameter to account for the zero-bias ME coupling in bilayers of the ferrite composites with PZT as discussed later. There are several avenues for the determination of H_A, such as direct measurements and from M vs H data, we utilized FMR results in combination with magnetization values to estimate H_A. Data on f_r vs H in Fig. 7 (and Fig. S5) were fitted to appropriate expression for f_r to determine the effective magnetization $4\pi M_{eff}= 4\pi M + H_A$, where $4\pi M$ is the magnetization and H_A is the magnetocrystalline anisotropy field. It is essential to note that $4\pi M$ is not the saturation magnetization since the M vs H in Fig.3 (and Fig.S3) clearly indicate that there is no saturation of M with H for several of the composites used in this study. We instead used the average value of $4\pi M$ for H-values for FMR profiles in Fig.5.

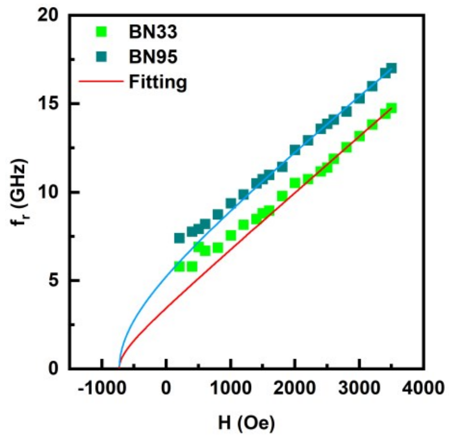

Figure 7. Fitting of the FMR data on f_r vs H to Eq. (1).

The resonance frequency f_r for FMR mode is given by the Kittel equation,

$$f_r = \gamma\left(\left(H + (N_z - N_x)4\pi M_{eff}\right)\left(H + \left(N_y - N_x\right)4\pi M_{eff}\right)\right)^{1/2} \quad (1)$$

where, γ is the gyromagnetic ratio, H is the in-plane external magnetic field along the x-direction, N_x, N_y and N_z are the demagnetization factors along the length, width and thickness of the platelet, respectively, and are given Table 1 for each of the composites in which FMR mode was observed. The data as in Fig.7 (and Supplementary Fig. S5) were fitted to Eq. (1) to determine $4\pi M_{eff}$. The Kittel equation in the presented form is, strictly speaking, applicable to the ferromagnetic samples of ellipsoidal shape, magnetized to saturation and with uniform static and dynamic magnetization. On the contrary, the samples presented in this investigation did not have ellipsoidal but a parallelepiped shape. That means, that even after an external magnetic field $H>N_x4\pi M$ was applied and domain structure was suppressed, the sample was still not in the uniformly magnetized state. There were regions of ferrite present (mostly around edges and corners [30]) where the magnetization deviates from the direction of bias magnetic field. Thus, an even larger H should be applied before the magnetic state of the sample becomes uniform and Kittel equation becomes applicable. Due to these reasons, we took only the high-frequency (and high-field) portion of the dependencies shown in Fig. 7 for the fitting with Kittel equation since to obtain most reliable fitting parameters.

Table 1. Demagnetization factors for BN composites.

Sample	Demagnetization Facotrs		
	N_x	Ny	N_z
BN33	0.11164	0.31851	0.56984
BN38	0.11238	0.32595	0.56167
BN41	0.10642	0.2778	0.61578
BN44	0.10168	0.30318	0.59514
BN47	0.11442	0.2892	0.59638
BN60	0.16197	031884	0.51919
BN75	0.19305	0.40187	0.40508
BN85	0.12413	0.22542	0.65045
BN95	0.10323	0.20369	0.69308
NFO	0.11812	0.40771	0.47417

Table 2. Fitting parameters for FMR and magnetic parameters for BNx composites. Gilbert damping constants are also given.

Sample	FMR Fitting parameters		Measured saturation magnetization, $4\pi M_s$ (kG)	H_A (kOe)	Coercive field (kOe)	Remanent Magnetization (M_r) (kG)	Gilbert damping coefficient calculation	
	γ (GHz/kOe)	$4\pi M_{eff}$ (kOe)					Frequency width (GHz)	Gilbert damping coefficient (α)
BN33	3.17	3.53	2.63	0.90	0.255	0.91	3.071	0.02450
BN38	3.26	3.46	2.68	0.78	0.161	0.77	3.042	0.02452
BN41	3.03	4.80	2.34	2.46	0.124	0.63	3.324	0.02491
BN44	2.96	5.30	2.88	2.42	0.114	0.49	3.35	0.02389
BN47	2.98	5.51	2.88	2.63	0.111	0.59	3.25	0.02354
BN60	2.61	10.07	2.75	7.32	0.089	0.73	2.739	0.01699
BN75	2.71	10.54	2.77	7.77	0.046	1.04	2.943	0.01911
BN85	2.98	7.49	2.92	4.57	0.034	0.73	2.535	0.01635
BN95	2.96	7.25	2.87	4.38	0.035	0.83	2.549	0.01613

Estimated values of the gyromagnetic ratio γ and $4\pi M_{eff}$ from the fits and the average values of $4\pi M$ for H = 1 kOe to 3.5 kOe (from M vs H data) are given in Table 2. The values of γ range from 3.17 GHz/kOe for x = 33 to 2.61 GHz/kOe for x = 0.60 that are comparable to 3.0 to 3.2 GHz/kOe reported for pure NFO [28,29]. The value of the anisotropy H_A estimated from FMR data are also given in Table 2 will at least have an error of 0.5 kOe. The anisotropy field H_A is positive for x = 33 -95, indicative of in-plane anisotropy for all the polycrystalline BNx composites with x=33-95. The anisotropy increases from ~ 0.90 kOe for x=33 to ~ 7.77 kOe for x=75. A further increase in x results in a decrease in H_A but the in-plane character of the anisotropy remains. One may therefore infer from these H_A -values that a majority of BaM crystallites in x = 33 -95 have a unique in-plane orientation leading to positive values of magnetic anisotropy. With increasing value of NFO content in x ≥ 33, the higher concentration of NFO appears to promote the growth of BaM crystallites with in-plane orientation for the c-axis and a net in-plane anisotropy field that reaches a maximum value for x = 75. Several reported efforts in the past on polycrystalline BaM mainly dealt with textured thin and thick films and showed, depending on the degree of texture, an out-of-plane H_A in the range 4.5 to 15 kOe [31,32]. In this work, however, the BaM component in composites results in overall effective in-plane anisotropy field.

We have also calculated the Gilbert damping coefficient (GDC) [33,34] of the composites by analyzing the FMR spectra of the samples. GDC is a dimensionless quantity which can be used as a measure of the losses in a ferromagnetic material. GDCs of the composites were calculated using the equation,

$$\alpha = \frac{\gamma \Delta H}{4\pi f_r} \qquad (2)$$

where, α is the damping coefficient, f_r is the resonance frequency, ΔH is the linewidth that was estimated from the FMR frequency-width for profiles in Fig.5 and γ is the gyromagnetic ratio. Estimated values are given in Table 2. Composites with x≤47 show GDC ~0.024 and we get a smaller GDC less than 0.02 for x≥60 and is indicative of a decrease in the losses in the composites as the NFO increases. The composites seem to have a much larger damping coefficient compared to pure and dopedNFO [34,35] but smaller than the GDC of BaM [36].

3.4 Magneto-electric effects in the BNx-PZT bilayers

The strength of ME coupling was measured in bilayers of the composites and vendor supplied PZT (PZT850, American Piezo Ceramics, USA). Ferrite platelets of approximate lateral dimensions 5 mm × 10 mm and thickness t = 0.3 – 0.5 mm were bonded to PZT with 20 μm thick layer of a fast-dry epoxy. The ME voltage coefficient (MEVC) was measured for two different orientations of the applied magnetic fields: (i) α_{31} for the DC filed H and ac field H_{ac} both parallel to each other and along the length of the sample (direction-1) and the induced voltage I measured across the thickness of PZT (direction-3)(ii) α_{33} for the magnetic fields applied perpendicular to the sample plane (direction -3) and induced voltage measured across PZT thickness. The MEVC is given by $\alpha = V_3/(H_{ac}\, t)$, where V_3 is the strain induced ac voltage measured across PZT. The ME coefficients were measured at low frequencies as well as at mechanical resonances in the bilayers.

Figure 8 (and Figure S6 in the supplement) shows the H dependence of α_{31} for ac field at 100 Hz. The MEVC is directly proportional to the piezomagnetic coupling q = dλ/dH. The value of α_{31} increases with increase in H to a maximum. The maximum value of MEVC for BN5 is rather small due to low q-value for this BaM rich composite. With further increase in the NFO content in the composites, α_{31} increases to a maximum value

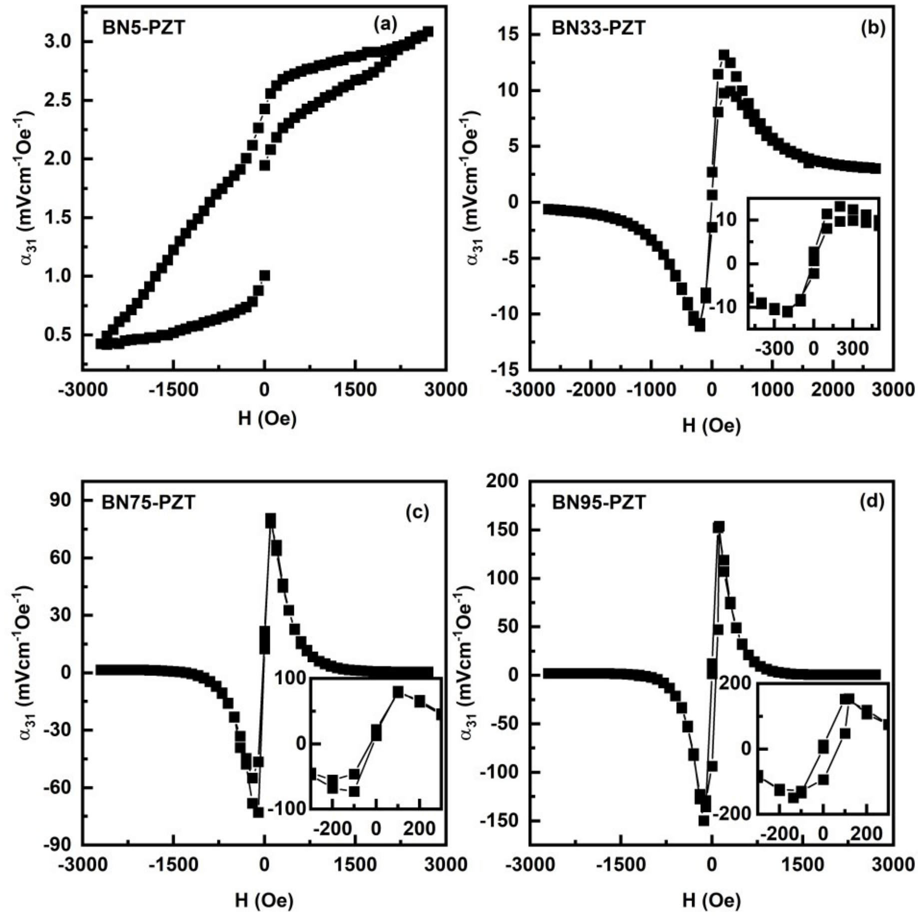

to

Figure 8. Variation of the ME voltage coefficient MEVC α_{31} with the magnetic field H for both ac field h and DC magnetic field H applied parallel to the ferrite-PZT bilayer for (a) BN5-PZT, (b) BN33-PZT, (c) BN75-PZT and (d) BN95-PZT.

of ~ 152 mV/cm Oe for BN95. Upon further increase in H, α_{31} in general decreases to a minimum for composites with x > 5. Bias field H dependence of α_{31} in Fig.8 essentially tracks the variation in q with H, reaches a maximum at the maximum in the slope of λ_{11} vs H, and drops to near zero when the magnetostriction (Fig.3) shows near saturation. Other significant features in the results from Figure 8 are as follows. (i) When H is decreased from ~ 3 kOe back to zero a hysteresis in α_{31} vs H is evident for all the BNx-PZT bilayers. (ii) Upon reversing the field H, a 180 deg phase shift (indicated by negative values for α_{31}) is observed in the ME voltage except for x=5. (iii) The bilayers show a finite remnant value for α_{31} at zero-bias and, as discussed later, is attributed to the built-in bias in BNx provided by the anisotropy field H_A.

Figure 9 shows results of MEVC measurements for the magnetic fields applied perpendicular to the bilayers of BNx-PZT (also shown in the supplement, Fig.S6). The variation in MEVC has similar hysteresis and remanence as for the in-plane magnetic fields. However, the following features in α_{33} vs H differ from the dependence of MEVC for in-plane magnetic fields. (i) Overall MEVC values are smaller in Fig. 9 since demagnetization factors reduce both the dc and ac magnetic fields. (ii) the decrease in MEVC for H > 1.5 kOe is relatively small compared to α_{31} vs H. (iii) Data in Fig.9 for BN95-PZT bilayers shows a reversal in the sign of for H > 0.75 kOe for both positive and negative H.

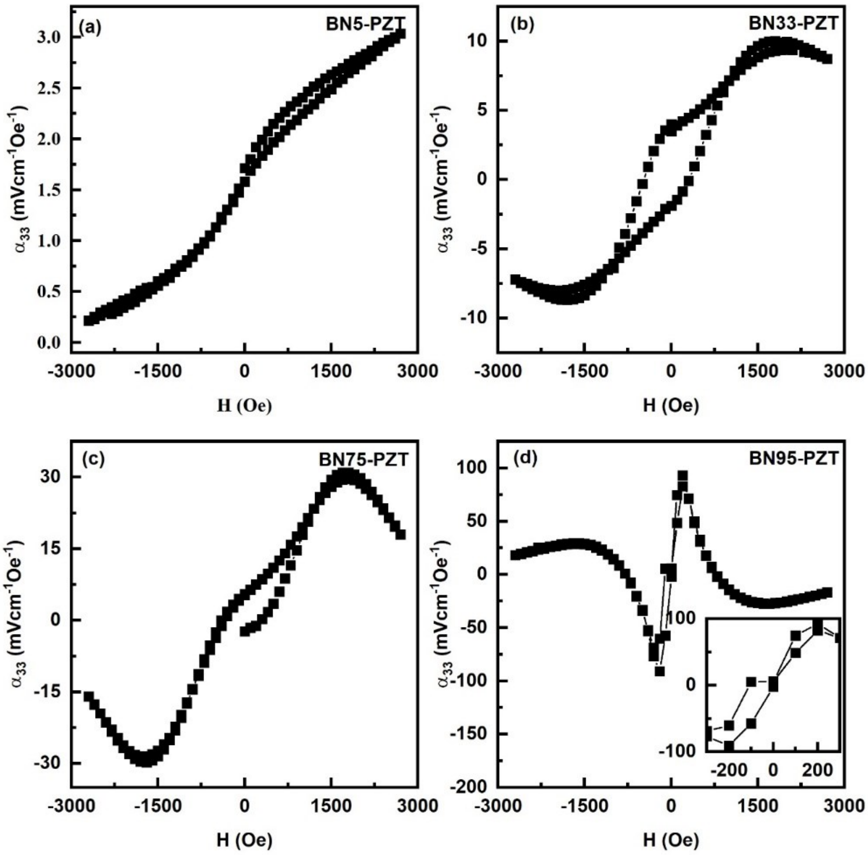

Figure 9. Similar MEVC α_{33} vs H data as in Figure 7 for H and h applied perpendicular to the sample plane for bilayers of (a) BN5-PZT, (b) BN33-PZT, (c) BN75-PZT and (d) BN95-PZT.

The strength of ME coupling in the bilayers was also characterized by measuring the ac magnetic field frequency f dependence of the MEVC at mechanical resonance modes. Prior to these measurements we obtained the electromechanical resonance (EMR) frequencies (f_r) for the composites by measuring the frequency dependence of the impedance with an LCR meter. Mode frequencies could not be obtained for BNx for x≤19, but we were able to determine the frequency of longitudinal resonance modes for higher x-values. MEVC α_{31}vs f under a bias field H =100 – 200 Oe for the bilayers are shown in Fig.10. One observes an increase in α_{31} with increasing f and a sharp peak in its value at f_r ~ 55 – 75 kHz. We were able to identify f_r with the longitudinal EMR mode from the known composite dimensions. For x=33 the figure shows a fine structure with a double peak in the α_{31}vs f profile with values of 147 mV/cm Oe at 72.9 kHz and 132 mV/cm Oe at 73.2 kHz. Bilayers of BNx-PZT with x>33 have a single peak in the profiles and BN95-PZT shows the highest value of α_{31}=992 mVcm^{-1}Oe^{-1} at 59 kHz. One observes a significant enhancement in the ME coefficients at f_r compared to values at 100 Hz (Fig.8), and for example, by a factor 36 for x=41. The highest Q-factor obtained from this data is found to be 130.4 for BN44. BN41 also has a large Q-factor of 118. After BN44 the Q-factor reduced to 75 at BN60. We discuss the results of these ME measurements in the following section.

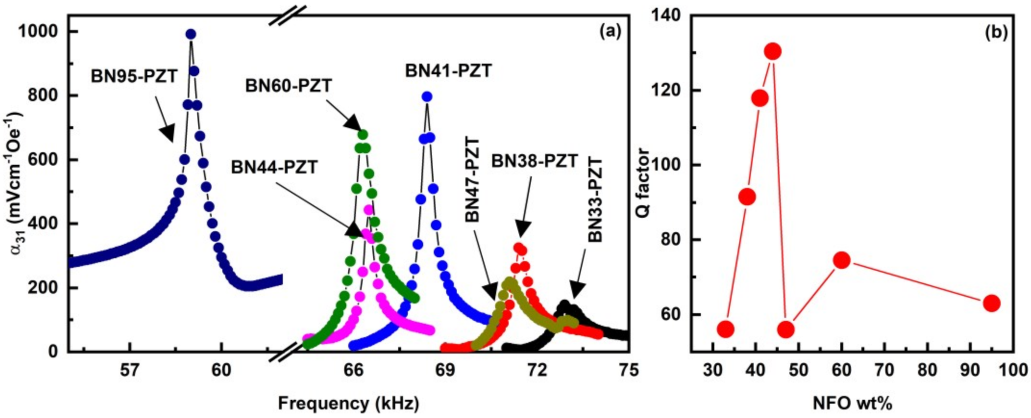

Figure 10. (a) Frequency dependence of ME coefficient α_{31} for bilayer of BNx-PZT. The peak values of MEVC occur at longitudinal mechanical resonance frequency in the samples. (b) Q-factor as a function of NFO weight fraction of BNx composites from the resonance ME response.

4. Discussions

It is evident from the results of this study that (i) it is possible to synthesize composites of spinel and M-type hexagonal ferrites free of ferromagnetic impurity phases, (ii) the composites, depending on the amount of BaM, have a moderately high induced planar anisotropy in all compositions, and (iii) the magnetostriction is quiet small for BaM rich composites, but increases significantly with increasing NFO content although the piezomagnetic coefficient q is rather small in all of the composites due to slow increase in λ with H compared to pure NFO.

It is interesting to note that the coercive field estimated from M vs H data for the BNx composites remains well under 0.3 kOe for all compositions from x=33-95. The coercive field gradually increases from 35 Oe for BN33 to 256 Oe for BN95. BN75, the material having highest anisotropy field of 7.77 kOe have a coercive field ~45 Oe. It is also important to note that the highest remanent magnetization is also obtained for BN75 having highest anisotropy. The anisotropy acts as a driving force giving rise to a remanent magnetization for all BNx samples and a zero-bias MEVC in bilayers with PZT. All the BNx samples remains soft magnetic material with coercive field less than 300 Oe with no significant hysteresis loss for x=33-95. This value of coercive field is well below the coercive field of pure polycrystalline BaM which possesses a large coercive field ~5 kOe. In the composites the stabilization of the BaM grains (Fig. 2) does not seem to increase the coercive field.

It is also clear from the results of ME measurements in Figs.8-10 that the bilayers of BNx and PZT show MEVC that are much higher than reported values for M-type hexaferrite-PZT bilayers [37], but smaller than for NFO-PZT [38]. Under optimum value of H, the highest MEVC are α_{31} = 152 mV/cm Oe and α_{33} = 90 mV/cm Oe, both for BN95-PZT. These values, however, are relatively small due to the weak piezomagnetic coupling strengths in BNx compared to nickel ferrite or nickel zinc ferrite based layered composites with PZT [34,39].

A key and primary objective of this work was to synthesize a ferromagnetic oxide with a moderately large H_A and high magnetostriction and piezomagnetic coupling for use with PZT to achieve ME coupling in the absence of an external bias magnetic field. It is worth noting that this goal was indeed accomplished. Bilayers of BNx-PZT used in this study do show a zero-bias MEVC (Figure S7 in the supplement). Bilayer of BN75-PZT shows the highest α_{31}=22 mV/cm Oe at zero-bias and BN85-PZT bilayer shows highest α_{33}=9 mV/cm Oe at zero-bias. It is noteworthy that the remanent magnetization of 1.04 kG for BN75 is the highest for the composites (Table 2). Strategies employed in the past to realize zero-bias ME effects included the use of an external stimuli or a functionally graded composites, either in magnetization or in composition, etc [7-17]. The use of an easy to synthesize composite of a spinel ferrite and hexaferrite in this work for zero-bias ME effect makes this method more viable than others. There are reports wherein composites consisting of NFO and PZT show large ME coefficient of 460 mV/cm Oe for bilayers and ~1200 mV/cm Oe for multilayers [40]. The MEVC at resonance in these systems was as high as ~1 V/cm Oe [41]. Modified NFO and PZT multilayers even showed a higher ME coefficient [42]. But there is hardly any evidence for ME coupling zero-bias effect in these composites [37-43].

Due to very low magnetostriction BaM is not suitable for strong direct ME coupling, but the very high uniaxial anisotropic field in the system is utilized in this work. Even though BaM grains in our BNx composites are expected to be completely randomized leading to a net zero the anisotropic field, the increase in the NFO content in BNx seems to promote the growth BaM grains with in-plane c-axis and a net in-plane anisotropy field.

Finally, we compare the zero-bias MEVC values with results reported in the past. Use of a nickel zinc ferrite graded either in magnetization or composition in a bilayer with PZT resulted in a zero-bias MEVC of 37 mV/cm Oe. Electric field induced bending vibration mode generated zero-bias ME effect in lead free system show a MEVC ~30 mV/cm^{-} Oe [9]. Low field hysteresis based zero-bias effect also showed a value of ~60 $mV/cm^{-} Oe^{-}$ [16]. In our work we have obtained zero-bias ME coefficient ~22 $mV/cm^{-}Oe^{-}$ for BN75-PZT bilayer which is comparable to the earlier report [10]. The zero-bias ME response in our study could be improved with the use of composites of NFO and M-type strontium ferrite (SrM) or Al substituted SrM or BaM with higher λ than pure BaM. Substituted BaM or SrM may be good choices as they also have anisotropic fields as high as ~30kG [43].

5. Conclusion

In this work we have successfully synthesized a novel ferrimagnetic composite consisting of (i) nickel ferrite with high magnetostriction and (ii) M-type barium hexaferrite with very high magneto-crystalline anisotropy field. The aim was to use such a high-q and high-H_A composite to achieve strong ME coupling in the absence of a bias magnetic field in a bilayer with PZT. BNx composites with x = 5-95 wt.% had high q for NFO rich compositions and in-plane H_A as high as 7.77 kOe for x=75. ME voltage coefficient measurements at low frequencies and at resonance modes showed moderately strong ME coupling at zero bias for samples with NFO content ≥33 wt.%. The highest zero bias MEVC of 21.82 $mVcm^{-1}Oe^{-1}$ was obtained for BN75-PZT bilayers wherein BN75 also possesses the highest anisotropy. BN41-PZT shows MEVC ~800 $mVcm^{-1}Oe^{-1}$ at electromechanical resonance at 68.4 kHz. The BNx-PZT composites have the potential for use in energy harvesting and sensor technologies.

Supplementary Materials: Fig.S-1: X-ray diffraction patterns of BNx composites. All composites bear the signatures of NFO and BaM. We have plotted the stick patterns for NFO (PDF No. 00-003-0875) and BaM (PDF No. 00-007-0276) in the bottom pane to visualise the one-to-one correspondence of the Braggs' positions of each phase to the respective NFO and BaM lines. Fig.S-2: SEM images of BNx (x=5, 9, 13, 33, 38, 41, 44, 47, 60, 75, 85 and 95). Hexagonal BaM grains develop with increasing grain size as the NFO content increases. After BN41 the BaM grains deteriorate in size. SEM images of pure BaM and NFO are also shown at the bottom. Fig.S-3: S_{21} vs f profiles showing FMR and magneto-dielectric modes in BNx composites at selected bias magnetic fields. Fig. S-4. Ferromagnetic resonance frequency of (a) NFO part and (b) magneto-dielectric mode frequencies of BNx composites are plotted as function of external magnetic field (H). (c-l) Kittel equation fit of the NFO part of FMR data of the samples BN33, BN38, BN41, BN44, BN47, BN60, BN75, BN85, BN95 an NFO respectively. Fig. S-5. Magnetization vs. magnetic field data for BN composites. Fig. S6. MEVC at for BNx-PZT bilayers for in-plane magnetic fields (left) and out-of-plane magnetic fields (right). Fig. S-7. Zero bias and maximum achievable ME coefficient for BNx-PZT bilayers in transverse and longitudinal modes.

Author Contributions: All authors contributed to this work. Sample synthesis: S.S., S. A., R. B., Data curation: S.S., S. A., and R. B., T. S., J. P., M.P., and G.S; formal analysis: S.S., M.P., funding acquisition: M.P., M.J., G.S and M.R.P, project administration: M.P., M.J., G.S., and M.R.P., original draft preparation: S.S., and G.S. All authors have read and agreed to the published version of the manuscript.

Funding: The research at Oakland University was supported by grants from the National Science Foundation (NSF) (ECCS-1923732, ECCS-EAGER-2236879, DMR-1808892) and the Air Force Office of Scientific Research (AFOSR) Award No. FA9550-20-1-0114. The research at the Taras Shevchenko National University of Kyiv was supported by the Ministry of Education and Science of Ukraine, Project No. 0122U001908. Efforts at the University of Connecticut were supported by the NSF (ECCS-EAGER-2236879). The research at AFRL was partially supported by the AFOSR Award No. FA9550-23RXCOR001.

Data Availability Statement: Data are available from the corresponding author upon reasonable request.

Conflicts of Interest: The authors declare no conflict of interest.

References

1. Vopson, M.M. Fundamentals of Multiferroic Materials and Their Possible Applications. *Crit. Rev. Solid State Mater. Sci.* **2015**, *40*, 223-250.
2. Fiebig, M.; Lottermoser, T.; Meier, D.; Trassin, M. The evolution of multiferroics. *Nat. Rev. Mater.* **2016**, *1*, 16046.
3. Spaldin, N.A.; Ramesh, R. Advances in magnetoelectric multiferroics. *Nat. Mater.* **2019**, *18*, 203-212.
4. Nan, C.-W.; Bichurin, M.I.; Dong, S.; Viehland, D.; Srinivasan, G. *J. Appl. Phys.* **2008**, *103*, 031101.
5. Eerenstein, W.; Mathur, N.D.; Scott, J.F. Multiferroic and magnetoelectric materials. *Nature*, **2006**, *442*, 759-765.
6. Caicedo, J.M.; Zapata, J.A.; Gómez, M.E.; Prieto, P. Magnetoelectric coefficient in $BiFeO_3$ compounds. *J. Appl. Phys.* **2008**, *103*, 07E306.
7. Zhou, Y.; Maurya, D.; Yan, Y.; Srinivasan, G.; Quandt, E.; Priya, S. Self-Biased Magnetoelectric Composites: An Overview and Future Perspectives. *Energy Harvest. Syst.* **2016**, *3*, 1-42
8. Liu, S.; Liao, S.; Wei, K.; Deng, L.; Zhao, L.; Zou, H. Self-biased magnetoelectric composite for energy harvesting. *Battery Energy*, **2023**, *2*, 20230005.
9. Yang, S.C.; Cho, K.-H.; Park, C.-S.; Priya, S. Self-biased converse magnetoelectric effect. *Appl. Phys. Lett.* **2011**, *99*, 202904.
10. Mandal, S.K.; Sreenivasulu, G.; Petrov, V.M.; Srinivasan, G. Flexural deformation in a compositionally stepped ferrite and magnetoelectric effects in a composite with piezoelectrics. *Appl. Phys. Lett.* **2010**, *96*, 9916.
11. Mandal, S.K.; Sreenivasulu, G.; Petrov, V.M.; Srinivasan, G. Magnetization-graded multiferroic composite and magnetoelectric effects at zero bias. *Phys. Rev. B* **2011**, *84*, 014432.
12. Sreenivasulu, G.; Mandal, S.K.; Bandekar, S.; Petrov, V.M.; Srinivasan, G. Low-Frequency and Resonance Magnetoelectric Effects in Piezoelectric and Functionally Stepped Ferromagnetic Layered Composites. *Phys. Rev. B* **2011**, *84*, 144426.
13. Laletin, U.; Sreenivasulu, G.; Petrov, V.M.; Garg, T.; Kulkarni, A.R.; Venkataramani, N.; Srinivasan, G. Hysteresis and remanence in magnetoelectric effects in functionally graded magnetostrictive-piezoelectric layered composites. *Phys. Rev. B* **2012**, *85*, 104404.
14. Lage, E.; Kirchhof, C.; Hrkac, V.; Kienle, L.; Jahns, R.; Knöchel, R.; Quandt, E.; Meyners, D. Exchange biasing of magnetoelectric composites. *Nature Mater.* **2012**, *11*, 523.
15. Borisov, P.; Hochstrat, A.; Chen, X.; Kleemann, W; Binek, C. Magnetoelectric switching of exchange bias. Phys. Rev. Lett. 94, 117203 (2005).
16. Zhou, Y.; Yang, S.C.; Apo, D.J.; Maurya, D.; Priya, S.; Tunable self-biased magnetoelectric response in homogenous laminates, *Appl. Phys. Lett.* **2012**, 101, 232905.
17. Yan, Y.; Zhou, Y.; Priya, S. Giant Self-Biased Magnetoelectric Coupling in Co-fired Textured Layered Composites. *Appl. Phys. Lett.* **2013**, *102*, 052907.
18. Huang, T.; Becerra, L.; Gensbittel, A.; Zheng, Y.; Talleb, H.; Salas, U.A.; Ren, Z.; Marangolo, M.; Self-Biased Magnetoelectric Ni/$LiNbO_3$/Ni Trilayers for Body-Embedded Electronic Energy Harvesters, *Phys. Rev. Appl.* **2023**, *20*, 034059.
19. Wu, J.; Du, Y.; Xu, Y.; Qiao, J.; Qu, Y.; Wang, Z.; Dong, S.; Hu, Z.; Liu, M. Self-Biased Magnetoelectric Sensor Operating in d_{36} Face-Shear Mode, *IEEE Sensors Journal*. **2023**, *23*, 22366.
20. Annapureddy, V.; Park, S.H.; Song, H.; Ryu, J, Tunable self-biased magnetoelectric effect in magnetization-graded magnetoelectric composites, *J. Alloy. Comp.* **2023**, *957*, 170121.
21. Aubert, A.; Loyau, V.; Mazaleyrat, F.; LoBu, M. Investigation of Piezomagnetism in Nickel Ferrite. *IEEE Trans. Magn.* **2021**, *57*, 2501105.
22. U. Topal, Factors influencing the remanent properties of hard magnetic barium ferrites: Impurity phases and grain sizes, *J. Magn.Magn. Mater.* **320**, 331-335 (2008)
23. Dudziak, S.; Ryżyńska, Z.; Bielan, Z.; Ryl, J.; Klimczuk, T.; Zielińska-Jurek, A. Pseudo-superparamagnetic behaviour of barium hexaferrite particles, *RSC Adv.* **2020**, *10*, 18784.
24. An, G.-H.; Hwang, T.-Y.; Kim, J.; Kim, J.B.; Kang, N.; Jeon, K.-W.; Kang, M.; Cho, Y.-H. Novel method for low temperature sintering of barium hexaferrite with magnetic easy-axis alignment, **2014**, *J. Euro. Ceram. Soc. 34*, 1227-1233.

25. Anantharamaiah, P.N.; Prerna Rao, B.; Shashanka, H.M.; Chelvane, J.A.; Khopkar, V.; Sahoo, B. Role of Mg^{2+} and In^{3+} substitution on magnetic, magnetostrictive and dielectric properties of $NiFe_2O_4$ ceramics derived from nanopowders, **2021**, *Phys. Chem. Chem. Phys. 23*, 1694.
26. Licei, F.; Rinaldi, S. Magnetostriction of some hexagonal ferrites. *J. Appl. Phys.* **1981**, *52*, 2442-2443.
27. Sheen, J. Comparisons of microwave dielectric property measurements by transmission/reflection techniques and resonance techniques, **2009**, *Meas. Sci. Technol. 20*, 042001.
28. Landolt-Bornstein; Numerical data and functional relationships in science and technology, Group III, Crystal and Solid State Physics, vol 4(b), Magnetic and Other Properties of Oxides, eds. K.-H. Hellwege and A. M. Springer, Springer-Verlag, New York, 1970.
29. Naiden, E.P.; Zhuravlev, V.A.; Minin, R.V.; Itin, V.I.; Korovin, E.Y. Static and dynamic magnetic properties of nanosized barium hexaferrite powders prepared by the sol-gel combustion method. *Russ. Phys. Journal*, **2015**, *58*, 125.
30. Joseph, R.I.; Schlömann, E. Demagnetizing Field in Nonellipsoidal Bodies. *J. Appl. Phys.* **1965**, 36, 1579.
31. Nie, Y.; Harward, I.; Balin, K.; Beaubien, A.; Celinski, Z. Preparation and characterization of barium hexagonal ferrite thin films on a Pt template. *J. Appl. Phys.* **2010**, *107*, 073903.
32. Wu, M. M-type barium hexagonal ferrite films. Rijeka: InTech, 2012.
33. Gilbert, T.L.; A Phenomenological Theory of Damping in Ferromagnetic Materials, *IEEE Trans. Magn.* **2004**, *40*, 3443.
34. Robbennolt, S.; Sasaki, S.S.; Wallace, T.; Bartholomew, M.; Tolbert, S.H. Fabrication and magnetic properties of Sol-Gel derived NiZn ferrite thin films for microwave applications, *Adv. Mater. Lett.* **2018**, *9*, 345.
35. Lumetzberger, J.; Buchner, M.; Pile, S.; Ney, V.; Gaderbauer, W.; Daffé, N.; Moro, M.V.; Primetzhofer. D.; Lenz, K.; Ney, A.; Influence of structure and cation distribution on magnetic anisotropy and damping in Zn/Al doped nickel ferrites, *Phys. Rev. B* **2020**, *102*, 054402.
36. Sharma, V.; Kumari, S.; Kuanr, B.K. Rare earth doped M-type hexaferrites; ferromagnetic resonance and magnetization dynamics, *AIP Advances* **2018**, *8*, 056232.
37. Pan, Q.; Zhang, X.; Xia, B.; Chu, B. Magnetoelectric response in laminated $BaFe_{12}O_{19}$/Pb(Zr,Ti)O_3 composites, *J. Appl. Phys.* **2023**, *133*, 244101.
38. Zhai, J.; Cai, N.; Shi, Z.; Lin, Y.; Nan, C.-W.; Coupled magnetodielectric properties of laminated $PbZr_{0.53}Ti_{0.47}O_3$/$NiFe_2O_4$ ceramics, *J. Appl. Phys.* **2004**, *95*, 5685-5690.
39. Hong-Xia, C.; Qian, S.; Jia-yang, Y.; Yu, F.; Huang, S. Transverse Magnetoelectric effect in nickel zinc ferriteLead zirconate titanate layered composites. *Adv. Mater. Res.* **2015**, *1061-1062*, 184-188.
40. Srinivasan, G.; Rasmussen, E.T.; Gallegos, J.; Srinivasan, R.; Bokhan, Yu.I.; Laletin, V. M. Magnetoelectric bilayer and multilayer structures of magnetostrictive and piezoelectric oxides, **2001**, *Phys. Rev B 64*, 214408..
41. Wang, Y.; Yu, Y.; Zeng, M.; Wan, J.G.; Zhang, M.F. Liu, J.-M.; Nan, C.W. Numerical modeling of the magnetoelectric effect in magnetostrictive piezoelectric bilayers. Appl. Phys. A **2005**, *81*, 1197.
42. Cótica, L.F.; Betal, S.; Morrow, C.T.; Priya, S.; Guo, R.; Bhalla, A.S. Thermal effects in magnetoelectric properties of $NiFe_2O_4$/Pb($Zr_{0.52}Ti_{0.48}$)O_3/$NiFe_2O_4$ tri-layered composite. Integrated Ferroelectrics, **2016**, *176*, 203-209.
43. Röschmann, P.; Lemke, M.; Tolksdorf, W.; Welz, F. Anisotropy fields and FMR linewidth in single-crystal Al, Ga and Sc substituted hexagonal ferrites with M structure, **1984,** *Mater. Res. Bull. 19*, 385.